Chemical Reactions at the Graphitic Step-Edge: *Changes in Product Distribution of Catalytic Reactions as a Tool to Explore the Environment within Carbon Nanoreactors*.

Maria A. Lebedeva,[a,b] Thomas W. Chamberlain,[a,c] Alice Thomas,[a] Bradley E. Thomas,[a] Craig T. Stoppiello,[a] Evgeniya Volkova,[d] Mikhail Suyetin,[d] Andrei N. Khlobystov [a,e]*

[a] School of Chemistry, University of Nottingham, University Park, Nottingham, NG7 2RD,UK.

[b] Department of Materials, University of Oxford, 16 Parks Road, Oxford, OX1 3PH, UK.

[c] School of Chemistry, University of Leeds, Leeds, LS2 9JT, UK.

[d] Institute of Mechanics of Ural Branch of Russian Academy of Sciences, T. Baramzinoy St., 34, Izhevsk, 426067, Russian Federation.

[e] Nottingham Nanotechnology and Nanoscience Centre, University of Nottingham, University Park, Nottingham, NG7 2RD, UK.

e-mail: maria.lebedeva@materials.ox.ac.uk

Abstract

A series of explorative cross-coupling reactions have been developed to investigate the local nanoscale environment around catalytically active Pd(II)complexes encapsulated within hollow graphitised nanofiber (GNF). Two new fullerene-containing and fullerene-free Pd(II)Salen catalysts have been synthesised, and their activity and selectivity towards different substrates has been explored in nanoreactors. The catalysts not only show a significant increase in activity and stability upon heterogenisation at the graphitic step-edges inside the GNF channel, but also exhibit a change in selectivity affected by the confinement which alters the distribution of isomeric products of the reaction. Furthermore, the observed selectivity changes reveal unprecedented details regarding the location and orientation of the catalyst molecules

inside the GNF nanoreactor, inaccessible by any spectroscopic or microscopic techniques, thus shedding light on the precise reaction environment inside the molecular catalyst-GNF nanoreactor.

Keywords: nanoreactor, catalysis, fullerene, salen, cross-coupling

Introduction.

Performing chemical transformations in extremely confined environments is a powerful way of controlling the pathways of chemical reactions. This strategy is fully exploited in biological systems, such as enzymes, where the spatial confinement of the catalytic centre plays a crucial role in the catalytic cycle and leads to the formation of unique products. The same principle is utilised in artificial nanoreactors - nanosized porous structures capable of encapsulating small molecules and directing the subsequent chemical transformations which occur within pores or channels - structures commonly used include zeolites,[1] molecular containers,[2] mesoporous inorganic materials,[3] metal-organic frameworks (MOF),[4] various polymers,[5] and hollow carbon nanomaterials.[6] Carbon nanostructures (CNS) such as single walled- (SWNT), double walled- (DWNT) and multi walled carbon nanotubes (MWNT) as well as hollow graphitised carbon nanofibres (GNF) are ideal nanocontainers which possess outstanding mechanical, chemical and thermal stabilities and can readily encapsulate guest molecules, enabling chemical reactions to be performed in their internal channels.[6] The spatial confinement imposed by the nanoscale channels not only allows the formation of unique products such as linear fullerene polymers,[7] graphene nanoribbons,[8,9] narrow inorganic nanowires[10] and atomic chains[11] inaccessible by conventional synthetic methods, but can also direct well-known organic and inorganic reactions to modify their selectivity as compared to the bulk phase.[12]

Determination of the precise reaction environment inside a nanoreactor is an important challenge as it is essential to understand all aspects of how the catalyst functions, down to the molecular/atomic level, if total control of reactions is to be achieved. Understanding every aspect, including the chemical nature of the internal surfaces, the pore size and accessibility and, most importantly, the location of the catalytic centres and reactant molecules during catalysis, is vital. Achieving this requires the combination of complimentary spectroscopic and microscopic techniques. Some smaller molecular nanoreactors, such as coordination metal-organic polyhedra (MOP), can be studied via traditional spectroscopic methods such as nuclear magnetic resonance (NMR), UV/vis absorption spectroscopies, or X-ray diffraction (XRD) methods which monitor changes in the nanoreactor cage itself or indirectly by observing changes in the reactant molecules upon encapsulation.[13] Detailed studies of the application of such cages as nanoreactors reveal the unique role of the MOP nanocontainer in pre-organising the reactant molecules inside the pore via hydrophobic host-guest interactions.[14] For the majority of bigger inorganic nanoreactors, high resolution transmission electron microscopy (HRTEM) - a powerful technique which allows direct imaging of nanostructures - can give useful results regarding the nanoreactor inner environment. For instance, the shape, pore size and accessible window diameter of silica cage nanoreactors was studied by TEM revealing the cavity-enhanced cooperative catalytic performance of the metal-salen catalysts trapped inside the cages.[15] It is also possible to investigate the shape, size and location of individual catalyst nanoparticles (NPs) inside carbon nanotube (CNT) or graphitised nanofiber (GNF) nanoreactors.[16] Moreover, HRTEM can be utilised to obtain real-time imaging of chemical transformations which occur under electron beam irradiation, and thus provide direct confirmation of the location and orientation of the reactant molecules inside the nanoreactor, specific reaction pathways and the role that the nanoreactor plays. For instance, the transformation of coronene molecules axially stacked inside SWNT into graphene nanoribbons

can be directly observed in TEM highlighting the unique templating role of SWNT nanoreactor.[17] Although very powerful, utilisation of TEM is however limited to a small number of molecular or nanoparticulate structures which have sufficient stability under the e-beam. Whereas the majority of organic molecules and molecular catalysts used in traditional synthetic chemistry become rapidly damaged by electron beam irradiation,[17] and therefore hinder the investigation of the precise inner reaction environment.

In this study we explore a non-direct method to investigate the local reaction environment inside a molecular catalyst-graphitised nanofiber (GNF) nanoreactor. We utilise a series of well-known size and shape sensitive catalytic reactions which proceed via a well-established mechanism as a tool to probe the different reaction environments inside a GNF nanoreactor, and relate the observed activity and selectivity changes to the structure and the steric environment of the catalytic site. The Heck reaction – an arylhalide-arylalkene cross-coupling reaction catalysed by Pd catalysts [18] - gives a distribution of several isomeric coupling products, the selectivity of which depends strongly on the electronic and steric environment of the catalytic centre,[19] and is therefore an ideal reaction system to investigate the local reaction environment of catalyst materials. Variation of the size and shape of the reactant molecules by incorporating bulky planar and non-planar substituents, as well as modifying the size and shape of the catalyst molecule by using a square planar Pd(II)Salen complex and a modified Pd(II)Salen-C_{60}, in which a bulky, spherical C_{60} cage is appended to the otherwise identical Pd(II)Salen complex,[20] results in notable changes of the catalyst activity and selectivity. The observed product distribution in each case reveals both important information about the role that the GNF nanoreactor plays in the catalytic process and unprecedented detail regarding the location and orientation of the fullerene-containing and fullerene-free catalyst molecules inside the GNF unavailable by any spectroscopic or microscopic techniques.

Results and discussion

4

Materials preparation.

We prepared two Pd(II)Salen catalysts for the Heck reaction according to our previously reported procedure[20] (Figure 1), **1**, which contains a fullerene group to provide high affinity to the graphitic surface of the carbon nanoreactor, and **2**, which doesn't have the fullerene spacer group but has been shown to bind to the GNF nanoreactor through similar van der Waals interactions, albeit with less affinity.[20] We immobilised both **1** and **2** within the inner channel of GNF using a previously reported solution filling method to form two heterogeneous nanoreactor catalysts, **1**@GNF and **2**@GNF respectively.[21] The freshly annealed GNF were immersed into the saturated solution of the corresponding Pd(II)Salen catalyst, **1** or **2**, in THF followed by slow removal of the solvent under reduced pressure. The solvent was then refilled, and the procedure repeated several times until the formation of nearly colourless solution upon addition of THF was observed. The slow removal of the solvent during the filling process draws the solution, and thus the catalyst, into the internal channel of the GNF whilst simultaneously creating a supersaturated solution of **1** in which the formation of clusters of fullerene-containing **1** [22] is promoted. The adsorption of clusters of **1** to the inner surface of GNF, driven by strong interactions between the curved surface of the fullerene cages appended to the catalyst with the commensurately curved graphitic surface of the inner sidewall and step-edge of the GNF, has been previously reported to be remarkably strong for various fullerene-containing molecules.[23] Addition of a second portion of neat solvent is used to dissolve any catalyst material deposited on the outer surface of the GNF and then the solvent evaporation step is repeated to draw the redissolved catalyst inside the GNF. This process is repeated several times to ensure as much of the catalyst material as possible is removed from the outside of the GNF and deposited inside. The encapsulation process was accompanied by the gradual loss of colour of the solution upon each iteration resulting in the nearly colourless solution in the final step (usually the total of 5-6 iterations) (Figure S1 in the SI), indicating that the majority of

molecules of **1** have been encapsulated on the inner surface of GNF where the interaction between the molecule and the substrate is much stronger than on the outer surface.[24] Upon completion the resulting composite material was dried in vacuum and used as obtained in the further catalytic reactions. As the catalyst in non-volatile and at no point is any washing step or filtration step involved which would result in loss of the Pd(II) material the final catalyst loading of the composite corresponds to the full amount of molecular catalyst used in the initial step of the filling procedure. A catalyst loading of 1.5×10^{-4} mmol of the Pd complex catalyst per milligram of GNF was used in all filling experiments, achieving the same catalyst loading in all further catalytic studies.

The resulting composite materials were initially investigated by HRTEM, with the fullerene cages of the individual molecules of **1** (seen as discrete circles with the diameter of approx. 0.7 nm) clearly observed to bind preferentially to the step-edges in the inner channel of GNF, (Figure 1 c, d). Moreover, the local-probe energy dispersive X-ray spectroscopy (EDX) confirmed the presence of Pd centres in **1**@GNF (Figure 1 d), however the exact location and orientation of the Pd(II)Salen moiety in **1** relative to the step-edges cannot be visualised by HRTEM. In the case of **2**@GNF the presence of Pd is also confirmed by EDX indicating successful encapsulation of **2**, however the individual molecules cannot be visualised by HRTEM measurements. Importantly local probe EDX and HRTEM observed no sign of Pd on the outside of the GNF in either material.
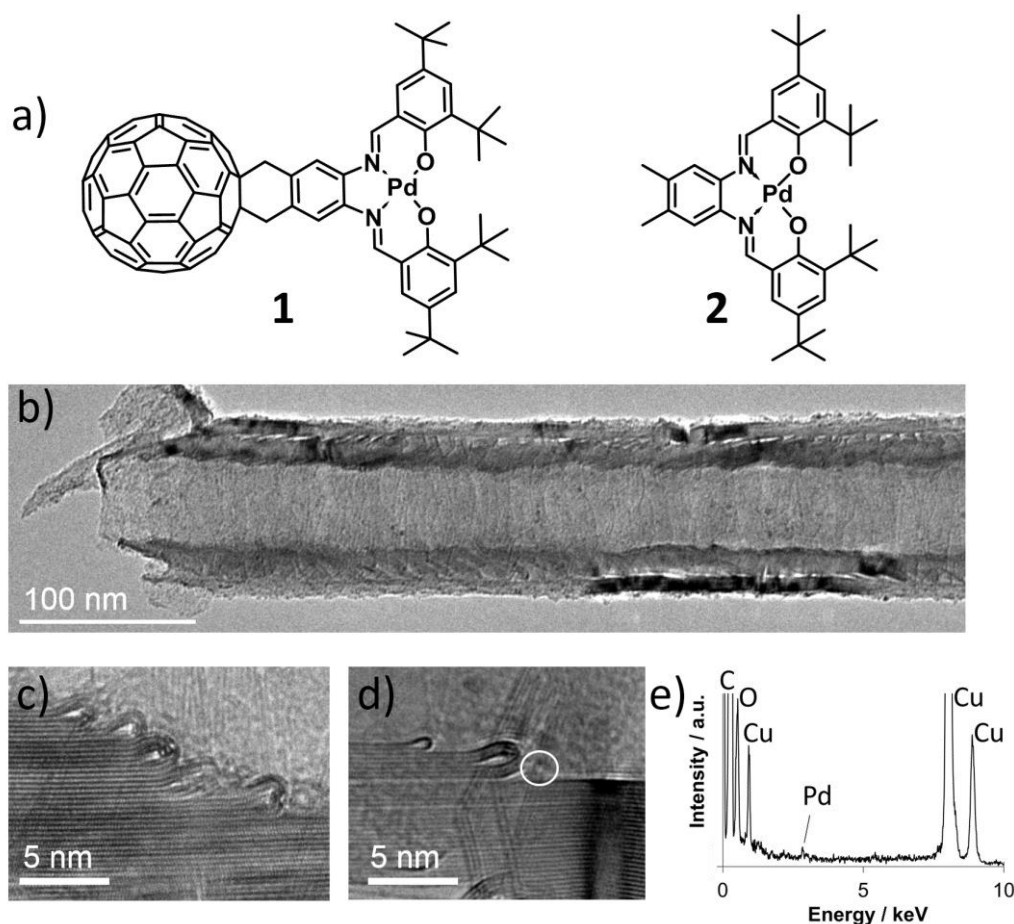
Figure 1. (a) Structural diagrams of the Pd(II)-(C$_{60}$Salen) (**1**) and Pd(II)(Salen) (**2**) complexes, (b) a TEM image of the **1**@GNF showing the cylindrical internal channel of the GNF, (c) and (d) high resolution TEM images of the step-edges inside the GNF nanoreactor in **1**@GNF show round-shaped molecules of **1** seen as discrete circles with the diameter of 0.7 nm (white circle), and (e) the EDX spectrum of **1**@GNF confirming the presence of Pd (N.B. Cu peaks are a result of the TEM sample grid).

Comparison of the infrared spectra of the composite **1**@GNF and **2**@GNF and the corresponding molecular catalysts (see Figure S2 in the SI) show that the spectrum is dominated by the C=C stretches of the GNF. The characteristic C-H stretches observed at 2800-3000 cm^{-1}, and CH=N observed at 1615 cm^{-1} in **1** and **2** [20] are very weak in the composite materials. The substantial quenching of these vibrations is due to the well-known shielding effect of the carbon nanostructures,[25] and the observed signals most likely originate from the

small number of catalyst molecules absorbed on the outer surface, as molecules located on the inner surface of GNF are shield from the IR beam.[25] Therefore it can be concluded that the majority of **1** and **2** are located inside the GNF and not adsorbed on the outer surface.

Catalytic studies.

Heterogeneous nanoreactors **1**@GNF and **2**@GNF were then utilised in several Heck reactions (referred to as "**1**@GNF" and "**2**@GNF"), and the results were compared with identical homogeneous reactions carried out in solution in the absence of GNFs, (referred to as "**1**" and "**2**"). As a control experiment, homogeneous reactions were also performed in solution with the addition of an equal amount of empty, as purchased GNF (referred to as "**1**+GNF" and "**2**+GNF") (Figure 2). These control reactions were intended to quantify the effect of having the GNF present in the reaction solution during the reaction. As inert carbon material it is unlikely that the GNF would play any significant role in the catalytic process (Table S1 in the SI), and the majority of the reactions would take place in solution between the catalyst and the reagents, however a small portion of the reagents and catalysts could potentially be adsorbed onto the GNF and thus a reaction could therefore theoretically take place on the outer surface of the GNF. Crucially the amount of material deposited on the inside of the GNFs under such conditions will be minimal as the concentrations of catalyst and reagents are significantly lower, and the temperature of the reaction is significantly higher than those used for the preparation of **1**@GNF and **2**@GNF catalysts.   Careful comparison of the catalyst activities and selectivities of the catalyst in each case enables the role of GNF support in the catalytic process to be determined and provides insight into the precise location and orientation of the catalytic centre in the GNF nanoreactor (Table 1).

We performed all Heck reactions under conditions typically used for Pd(II)Salen catalysed reactions.[26] All reactions were carried out in DMF in anaerobic atmosphere in the presence

of Na_2CO_3 at 140°C, and the resulting reaction mixtures were analysed by ^{1}H NMR spectroscopy. We initially varied the catalyst loadings in the reaction mixture and reaction times, with the best results obtained with 0.5 mol % catalyst after 90 h, and therefore used these conditions in all further experiments throughout the study (see SI file for the details and kinetic curves). We kept all other conditions (temperature, solvent, reagents ratio and nature of aryl halide) unaltered throughout the study to evaluate the effects of the nanoreactor environment and the size and shape of the reagents only. Each reaction was carried out in three different environments; in solution under homogeneous conditions, in solution but with the addition of empty GNF, the outer walls of which could potentially provide a smooth surface for the reaction, and under heterogeneous conditions within the GNF at the internal step-edge, Figure 2). The choice of reactants included unsubstituted bromobenzene and styrene; styrene and both 1-bromonaphthalene and 1-bromopyrene, both of which contain a larger planar aromatic group; bromobenzene and both 4-*tert*-butyl styrene and 4-methoxystyrene, both of which contain a bulky non-planar tertiary butyl or methoxy group in the para- position (Table 1). Reactions between styrene and 9-bromoanthracene,[27] 1-vinyl naphthalene and bromobenzene, and styrene and 1-bromo-4-*tert*-butylbenzene were also attempted, however resulted in poor conversions and therefore are not discussed any further (see SI for further detail).
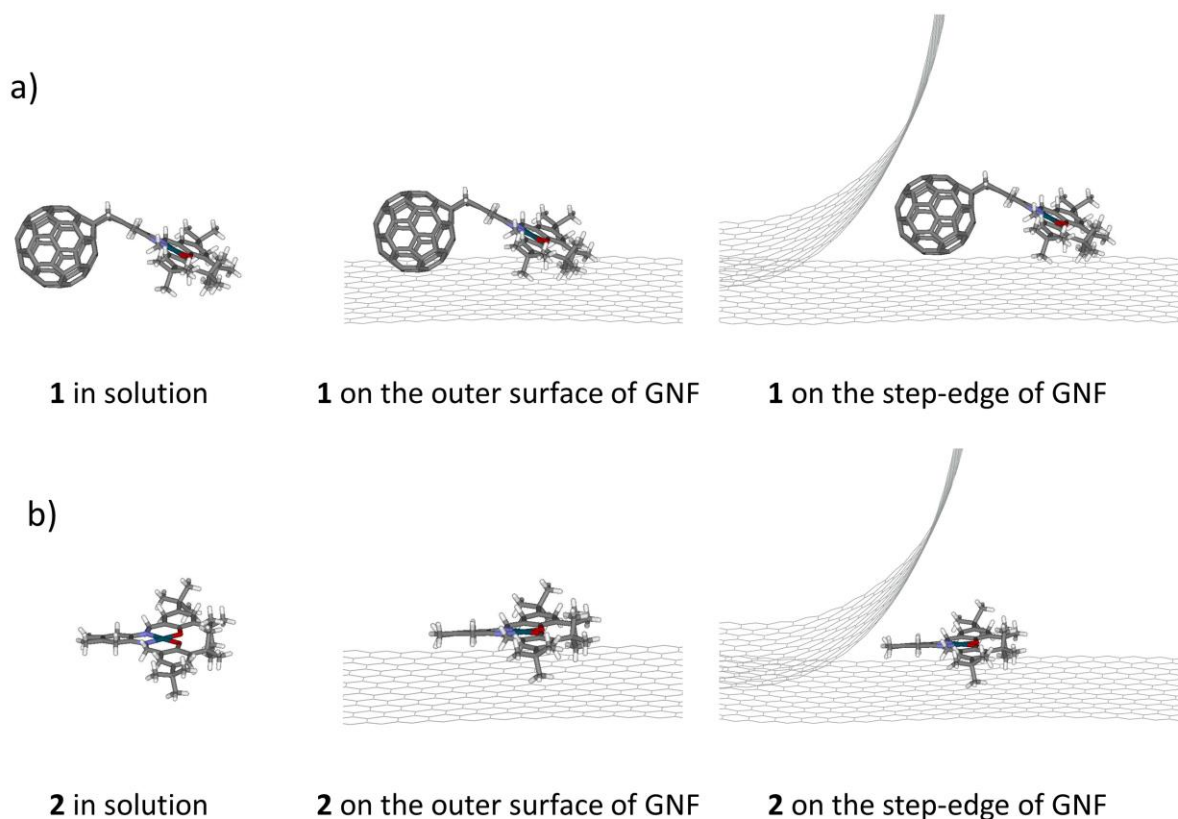
a)

1 in solution   **1** on the outer surface of GNF   **1** on the step-edge of GNF

b)

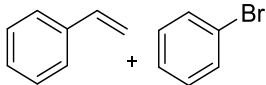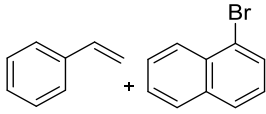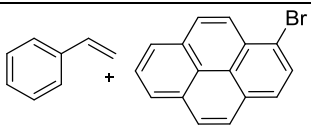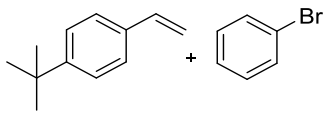**2** in solution   **2** on the outer surface of GNF   **2** on the step-edge of GNF

Figure 2. Schematic representations of molecules of **1** (a) and **2** (b) in solution (left), in solution with the addition of GNF, the outer surface of which could potentially provide a smooth surface for the molecules to adsorb (middle) and at the step-edge of a GNF (right) showing no steric restrictions of the catalytic centre in solution, steric restrictions from underneath on the surface of the GNF and steric restriction from two sides on the step-edge of the GNF.
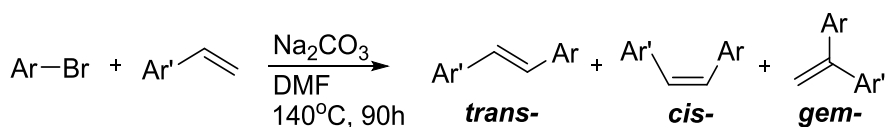
Scheme 1. Heck reaction between aryl bromide and aryl alkene resulting in the formation of *trans-*, *cis-* and *gem-* coupling products.

Table 1. Conversion, TON/TOF and selectivities towards *trans-*, *cis-* and *gem-* coupling products in the Heck reaction between aryl alkenes and aryl bromides catalysed by **1** or **2** under homogeneous or heterogeneous conditions. All yields determined by ^{1}H NMR as averages of 3 experiments, with an experimental error of $\pm$ 2 %.

Reagents	Catalyst	Conversion / %	TON[a]	TOF[b]	Selectivity / %		
					trans	cis	gem
styrene + bromobenzene	1	38	79	0.84	98	2	0
	1+GNF	35	70	0.78	93	1	5
	1@GNF	49	98	1.09	93	0	7
	2	18	36	0.4	89	5	6
	2+GNF	15	30	0.33	88	4	8
	2@GNF	31	62	0.69	89	2	9
styrene + 1-bromonaphthalene	1	58	116	1.29	79	9	12
	1+GNF	59	118	1.31	80	9	11
	1@GNF	61	122	1.36	77	8	15
	2	30	60	0.67	87	5	8
	2+GNF	39	78	0.87	84	3	13
	2@GNF	63	126	1.4	63	15	22
styrene + 1-bromopyrene	1	88	176	1.95	95	0	5
	1@GNF	90	181	2.01	94	1	5
	2	81	163	1.81	96	0	4
	2+GNF	83	166	1.84	96	0	4
	2@GNF	93	186	2.07	92	1	8
4-tert-butylstyrene + bromobenzene	1	40	80	0.89	91	2	7
	1+GNF	45	90	1	92	3	5
	1@GNF	42	84	0.93	82	9	9
	2	31	62	0.69	90	6	4
	2+GNF	33	66	0.73	82	6	12
	2@GNF	19	38	0.42	70	19	11
4-methoxystyrene + bromobenzene	1	34	67	0.75	98	0	2
	1@GNF	37	74	0.83	95	1	3
	2	32	64	0.71	100	0	0
	2+GNF	19	39	0.43	98	0	2
	2@GNF	17	34	0.38	97	0	3

reaction conditions: DMF, 140 °C, 90 h, 0.5 mol. % catalyst

[a] TON determined as [mol product]/[mol catalyst]

[b] TOF determined as [mol product]/([mol catalyst]*hour)

The Heck reaction proceeds with moderate yields and gives three coupling products (Scheme 1 and Table 1). The activity of the fullerene containing catalyst, 1, in solution (38 % conversion) is more than double that of the non-fullerene catalyst, 2 (18 %), which is attributed to the electron withdrawing effect of the fullerene group.[20] When confined inside the GNF in a heterogeneous system, both catalysts show significant increase in conversion to 49 % and 31

% for **1**@GNF and **2**@GNF respectively. This is attributed to an increased local concentration of reactants within the nanoreactor, a well-known effect for carbon nanotubes and nanofibers, increasing rate of reaction.[16] The higher than bulk solution concentrations of the aromatic reactants surrounding the catalytic centres at the step-edges of the inner channel of GNF are due to favourable π-π interactions between the phenyl groups of the starting materials (bromobenzene and styrene) and the sp^2 hybridised carbon step-edges.[16] In contrast, when reactions are performed on the outer surface of GNFs, by adding unfilled GNFs to a solution of **1** or **2** under catalytic conditions, no enhancement in conversion is observed. Therefore it is concluded that under reaction conditions the catalyst molecules in both **1**@GNF and **2**@GNF remain inside the GNF near the step-edges where such local concentration effects are maximised.

This is further supported by the stability against leaching and recyclability of the catalysts (see SI file for details). Both tests confirm good stabilities of **1**@GNF and **2**@GNF indicating that the majority of the catalyst molecules remain on the GNF support during the catalytic process. These stabilities are comparable with other previously reported non-covalently immobilised Pd-containing catalysts for Heck reaction,[28] for which it has been previously shown that strong chemical bonding between the substrate and Pd catalyst is required to reach high stabilities towards recycling, whereas catalysts attached via non-covalent bonding typically show quick dissolution enhanced by polar solvents and high temperatures.[29]

Comparison of the selectivities of the reactions carried out in solution, on the GNF outer surface and on the GNF step-edge (Figure 2) shows preferential formation of *trans-* stilbene in each case, with small amounts of *cis*-stilbene and *geminal* coupling products formed (Table 1). A small gradual increase of selectivity towards geminal coupling product with increasing steric constraint may be noted for both **1** and **2** (however very small and close to the error of

measurements) which we tentatively assign to the effects of the graphitic surface and the GNF step-edge.

Because the relatively simple reactants, bromobenzene and styrene, do not possess significant steric bulk, they are not measurably affected by the GNF step-edges. To enhance the steric factors in the reaction mechanism and thus to emphasise the effects of nanoscale confinement, we introduced bulky substituents to the reactant molecules.

Effects of substituents.

The Heck reaction was carried out between styrene and 1-bromonaphthalene, and styrene and 1-bromopyrene (Scheme 1), both of which are expected to have higher affinities for the graphitic surface of the GNF than unsubstituted bromobenzene due to the larger π-system of the naphthyl and pyrenyl groups (Table 1); and between bromobenzene and 4-*tert*-butylstyrene, and bromobenzene and 4-methoxystyrene (Scheme 1), which contain bulky and non-planar *tert*-butyl or methoxy groups which will hinder interactions with graphitic surfaces and reduce the affinity of these reagents for graphitic surfaces (Table 1).

Introducing the different substituents affects both the yield and the selectivity of the reactions, and the observed changes can be correlated with electronic or steric effects which influence different parts of the catalytic cycle. The catalytic cycle of the general Heck reaction is well-understood, and the proposed scheme for the Pd(II)(Salen) (**2**) catalysed reaction is shown in Figure S11 in the SI file to support observed changes in the selectivity (see SI file for details). [30]

Introducing bulky substituents affects both the yield and the selectivity of the resultant reactions, see Table 1. In all cases the conversions in solution are higher compared to the unsubstituted starting materials showing 58 % and 30 % conversions for **1** and **2** respectively for 1-bromonaphthalene, 88 % and 81 % for **1** and **2** respectively for 1-bromopyrene, 40 % and

31 % for **1** and **2** respectively for the 4-*tert*-butylstyrene, and 34 % and 32 % for **1** and **2** respectively for 4-methoxystyrene (Table 1). This is related to the electronic nature of each functional group which affects the corresponding steps in the catalytic cycle. For example, the strength of the C-Br bond in the aryl bromide affects the rate of the oxidative addition (step II, Figure S7),[30] as the energy of C-Br bond dissociation in 1-bromonaphthalene is approximately 20 kJ/mol lower than in bromobenzene,[31] which results in enhanced yields of the coupling products for 1-bromonaphthalene. Similarly, the electron-donating nature of the *tert*-butyl group of 4-*tert*-butylstyrene, and the methoxy group in 4-methoxystyrene increases the electron density on the double bond of the styrene which promotes the formation of the π-complex with the Pd centre (step III, Figure S11), and therefore also enhances the conversion. Confinement of the catalyst on the GNF step-edge has a significant effect on its activity in each case. Conversion of 1-bromonaphthalene in the presence of **2** increases from 30 % in solution to 39 % in solution with the addition of GNF and to a remarkable 63 % on the GNF step-edges. Similarly, the conversion of 1-bromopyrene in the presence of **2** increases from 81 % in solution to a nearly quantitative 93 % when performed heterogeneously on the GNF step-edges. Indeed, the large aromatic surfaces of 1-bromonaphthalene and 1-bromopyrene mean higher affinities for the graphitic surface of the GNF, leading to an increase in the local concentration of the corresponding reactants in the vicinity of the GNF surface, particularly localised around the GNF step-edges where the metal centres are also located (Figure 4 b). This localised increase in concentration of reactants around the Pd centre results in a corresponding increase in the rate of reaction and rationalises the observed increase in activity of the catalyst material. Such effects have been reported extensively for a variety of reactions using different confined nanoparticle@carbon nanostructure catalysts.[16] Surprisingly, the conversions of 1-bromonaphthalene and 1-bromopyrene catalysed by **1** are largely unaffected by the GNF step-edges and show only minimal increases in conversion of 58 % in solution to 61 % inside

the GNF for 1-bromonaphthalene and from 88 % in solution to 90 % for 1-bromopyrene inside GNF.

In contrast, conversions of 4-*tert*-butylstyrene and 4-methoxystyrene in the presence of **2** are not enhanced by the GNF step-edges and show a decrease in conversion from 31 % in solution to 19 % heterogeneously for 4-*tert*-butylstyrene, and from 32 % to 17 % for 4-methoxystyrene. Indeed, it appears that when at least one reagent with a bulky non-planar group, such a *tert*-butyl or methoxy-, is present this inhibits the reagent from lying flat on the graphitic surface to maximise such pi-pi interactions, therefore no increase in local concentration is observed and thus no enhancement in the rate of reaction. In addition, the steric bulk of the *tert*-butyl or methoxy groups could all hinder the formation of the π-complex between the double bond of styrene and the Pd centre in close proximity to the step-edge (step III in the catalytic cycle, Figure S11) therefore decreasing the observed activity of the catalyst. Again this effect is not observed in the presence of the fullerene-containing **1** which shows a small increase in conversion from 40 % in solution to 42 % on the step-edges for 4-*tert*-butylstyrene and from 34 % to 37 % for 4-methoxystyrene (Table 1).

These observations suggest that confinement on the step-edge of GNF has different effects on the fullerene-containing, **1**, and fullerene-free, **2**, catalysts. TEM measurements combined with leaching and recyclability tests of **1**@GNF show that the molecules of **1** are located mainly on the step-edges inside the nanoreactor under catalytic conditions (Figure 1), therefore a difference in geometry and the orientation of **1** and **2** at the step-edge must play an important role. It is hypothesised that as **1** contains a fullerene group with a particular affinity for the graphitic step-edge, the complex is oriented inside GNF nanoreactor in such a way that the catalytic Pd centre is further away from the step-edge (Figure 2a) reducing the extent to which the reaction is influenced by the steric and electronic effects of the nanoreactor. In contrast, the

molecules of **2** are much smaller and flatter, and therefore located much closer to the step-edge where any steric constraints are maximised (Figure 2b).

The molecules of **1** can have several orientations on the step-edge which will result in different distances between the Pd(II) centre and the GNF step-edge (Figure 3). Geometry optimisation of **1**@GNF and **2**@GNF was performed using molecular mechanics simulations (experimental section and SI file) for **1** in two extreme conformations orientated perpendicular (Figure 3a) and parallel to the step-edge (Figure 3b), and revealed distances between the Pd centre and the step-edge of approximately 16 Å and 8 Å respectively (Table 2). The distance of 16 Å is large enough to preclude any electronic or steric effects of the step-edge on selectivity, whereas a distance of 8 Å may allow active participation of the step-edge in the catalytic process. The calculated binding energies of complex **1** to GNF in perpendicular and parallel orientations are both large indicating a favourable, stabilising interaction for both orientations, with the parallel configuration being more stable (-3.70 eV vs. -2.46 eV). It is therefore suggested that within the composite material there is a mixture of the two orientations, with the parallel configuration being the major and perpendicular configuration being the minor component. Experimental results however show only a small influence from the step edge, indicating that although the parallel configuration is more abundant, it is less catalytically active than the minor perpendicular configuration. Indeed, close examination of the optimised geometry of **1**@GNF reveals that the Pd centre in the parallel configuration is difficult to access because of the close proximity of the step-edge, and therefore it is more difficult for the bulky reagents such as 1-bromonaphthalene, 1-bromopyrene, 4-*tert*-butylstyrene and 4-methoxystyrene to bind in the addition steps of the catalytic cycle. This supports the observation of similar activities experimentally observed for **1** and **1**@GNF. Although the concentration of the aromatic reagents is higher inside the nanoreactor due to local concentration effects, only the much lower number of catalyst molecules in the perpendicular configuration are affected by this, and the

overall change in conversion is negligible. In contrast, the non-fullerene catalyst **2** shows a similar distance of approx. 8-10 Å in both perpendicular and parallel orientations (Figure 3c and d), and therefore the steric effects imposed by the step-edge are essentially independent of the geometry of **2@GNF**. Furthermore, the binding energies of **2** on the step-edge are up to 1.5 eV lower than that of **1** parallel to the step-edge but comparable to those of **1** perpendicular to the step-edge, and differ by only 0.09 eV between the two configurations.
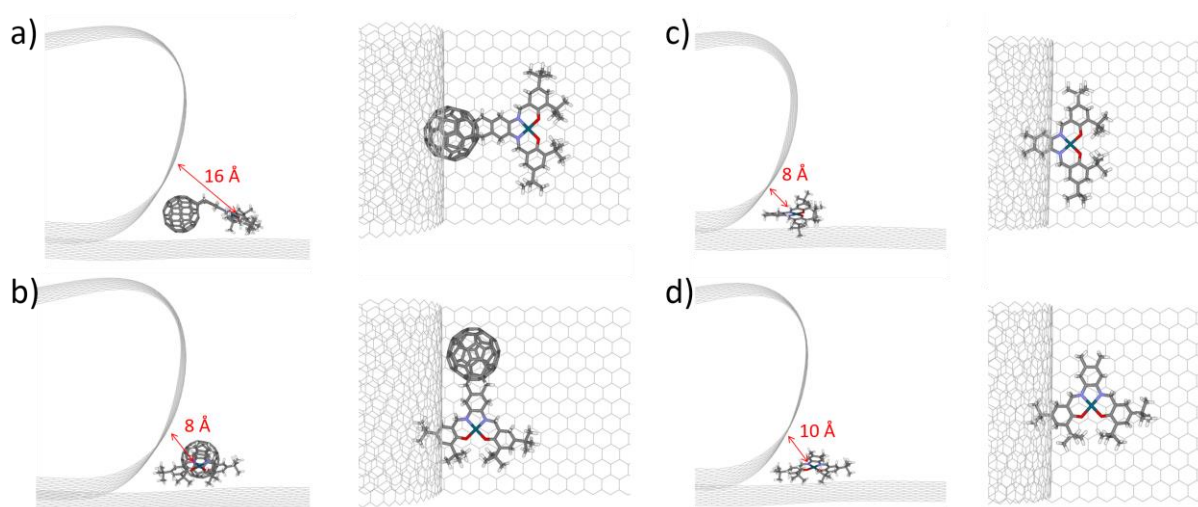
Figure 3. Molecular models of; a-b) Pd(II)(C$_{60}$Salen), **1**, on the step-edge of a GNF in two different orientations aligned perpendicular (a, side view and top view) or parallel (b, side view and top view) to the step-edge resulting in distances of approx. 16 Å and 8 Å between the Pd centre and the step-edge. c-d) Pd(II)(Salen), **2**, on the step-edge of a GNF in two different orientations aligned perpendicular (c, side view and top view) or parallel (d, side view and top view) to the step-edge resulting in similar distances of 8 and 10 Å between the Pd centre and the step-edge respectively.

Table 2. Geometry and binding energies of **1** and **2** on a GNF step-edge in different orientations obtained by molecular mechanics simulations (see experimental section and SI file for details).

Orientation	Pd to step-edge distance / Å	Binding energy / eV
1 ⊥ GNF	16	-2.46

1 ∥ GNF	8	-3.70
2 ⊥ GNF	8	-2.25
2 ∥ GNF	10	-2.16

The selectivity towards the geminal coupling product for 1-bromonaphthalene catalysed by **2** increases from 8 % in solution to a significant 22 % on the GNF step-edges. Similarly, the selectivity towards the geminal coupling product for 1-bromopyrene catalysed by **2** shows a two-fold increase from 4 % in solution to 8 % on the GNF step-edge (Table 1). This is related to the stabilisation of the geminal intermediate (step IIIb in the catalytic cycle, Figure S11) due to the significant contribution of the graphitic surface of GNF and the step-edge to the π-π stacking interactions in the intermediate (Figure 4). This supports our interpretation that the molecules of **2** are located preferentially close to the GNF step-edge during the catalytic process, and the graphitic surface of the step-edge participates actively in the catalytic process. The observations of selectivity changes for the 4-*tert*-butylstyrene and 4-methoxystyrene derivatives further support this hypothesis. The selectivity towards the geminal product increases from 4 % in solution to 12 % in solution with the addition of the GNF surface. However a similar selectivity of 11 % is observed on the step-edge which suggests a contribution from the underlying graphitic surface only in each case. Indeed, the steric bulk of the *tert*-butyl group precludes contribution of the step-edge from the top (Figure 4), which is also consistent with the changes in conversion of the 4-*tert*-butylstyrene discussed above. The same trend is observed for 4-methoxystyrene, although less profound (Table 1). Furthermore, a significant increase in the formation of the *cis*- isomer is observed for both 1-bromonaphthalene and 4-*tert*-butylstyrene in the presence of **2**@GNF showing a change from 5 % to 15 % and from 6 % to 19 % respectively. Confinement at the step-edge hinders the rotation in the corresponding intermediates containing bulky substituents (step VIa of the catalytic cycle) thus promoting the formation of the kinetic rather than the thermodynamic product.
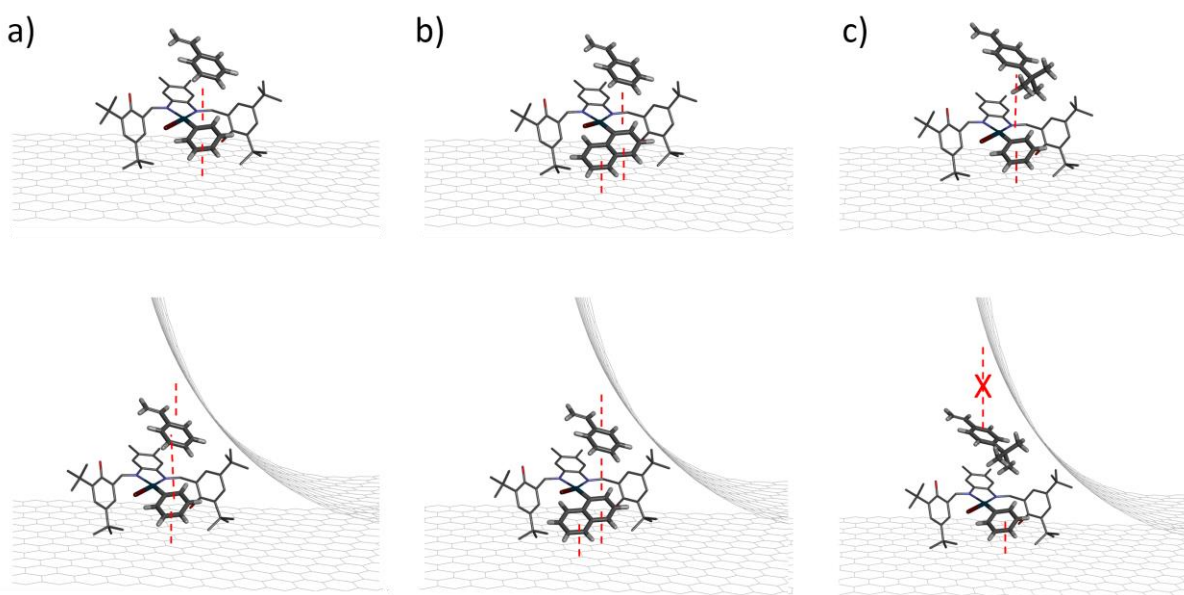
Figure 4. Molecular models of the stabilisation of the more sterically hindered geminal orientation of styrene in the π-complex with the Pd centre by the underlying graphitic surface (top) and by the step-edge of the GNF (bottom) for (a), styrene and bromobenzene, (b), styrene and 1-bromonaphthalene, indicating stronger interactions due to the larger aromatic surface of naphthyl group and (c), 4-*tert*-butyl styrene and bromobenzene showing how the steric bulk of the *tert*-butyl group hindering interactions with the step-edge. Red dashed lines indicate π-π stacking interactions.

For the fullerene-containing catalyst **1** only very small increases in geminal selectivity are observed in general, showing a change from 12 % in solution to 15 % on the step-edge for the 1-bromonaphthalene, from 7 % in solution to 9 % on the step-edge for the 4-*tert*-butylstyrene, from 2 % in solution to 3 % on the GNF step-edge for 4-methoxystyrene, and an unaltered selectivity of 5 % for 4-bromopyrene in both reactions. Furthermore, no noticeable change in selectivity towards the *cis*-isomer is observed for 1-bromonaphthalene, 1-bromopyrene or 4-methoxystyrene, and only a small increase from 2 % to 9 % is observed for the 4-*tert*-butylstyrene. This again confirms the hypothesis that the major parallel orientation has lower catalytic activity than the minor perpendicular orientation, and therefore the product

distribution observed in the catalytic reactions corresponds to that produced mainly by the perpendicular orientated catalyst (Figure 3) which is not affected by confinement on the step-edge and is almost identical to that in bulk solution.

Conclusions.

Encapsulation of Pd(II)Salen type complexes in GNF nanoreactors has been shown to increase their catalytic activities as compared to the bulk solution. Subtle changes in the environment around catalytic centres affect distribution of products catalysed by Pd(II)Salen, which allows probing the reaction environment inside GNF nanoreactors and study the effects of confinement on the catalytic activity. Detailed analysis of the product distribution of Heck cross-coupling reaction in combination with molecular mechanics calculations has a potential to reveal details of the precise geometry and orientation of catalyst molecules inside the nanoreactor.

TEM imaging and catalytic experiments demonstrated that both fullerene-containing and fullerene-free molecules are preferentially located on the step-edges in the internal channel of the GNF. Detailed comparison of yields and product distributions for different reactants with varied steric bulk, augmented by the theoretical calculations, showed that the catalyst molecules containing the fullerene anchor adopt two orientations with the orientation perpendicular to the 3 nm high graphitic step-edge being less abundant but more catalytically active than the parallel conformation due to the higher accessibility of the catalytic centre. In contrast, the fullerene-free catalyst is much smaller and located in close proximity to the step-edge side wall therefore being significantly affected by the confinement imposed by the graphitic step-edge. Furthermore, it is established that the GNF nanoreactor actively participates in the catalytic cycle changing the selectivity of the reaction towards less thermodynamically favoured products.

In the rapidly expanding field of spatially confined catalysis, it is becoming increasingly crucial to understand how the local nanoscale environment affect the reaction mechanisms. In this study we make a significant conceptual step to employ a well-known organic reaction as a probe for the environment within the carbon nanoreactor, obtaining details inaccessible by microscopy or spectroscopy, and therefore opening a new methodology to study in confinement and design bespoke nanoreactors for new products and materials.

Experimental

C_{60} was purchased from SES Research, USA. Compounds **1** and **2** were synthesised according to the previously reported procedures.[20] Graphitised carbon nanofibres (PR24, chemical vapour deposition, purchased from Pyrograf Products Inc) were thermally annealed at 400 °C for 40 minutes prior to use. All other reagents and solvents were purchased from Sigma-Aldrich and used without further purification. All reactions were carried out under Ar atmosphere and monitored by ^{1}H NMR spectroscopy. All catalytic reactions were performed three times, and the yields given are averages of the three experiments. ^{1}H NMR spectra were recorded using Bruker DPX 400 spectrometer. Infra-red spectra were measured using a Nicolet Avatar 380 FT-IR spectrometer over the range 400-4000 cm^{-1}.

HRTEM characterisation.

HRTEM imaging was performed using a JEOL 2100F transmission electron microscope (field emission electron gun, information limit 0.19 nm) using an accelerating voltage of 200 kV. TEM specimens were prepared by casting several drops of a methanolic suspension of **1**@GNF or **2**@GNF onto a copper TEM specimen grid mounted "lacey" carbon film and dried under a stream of nitrogen. EDX spectra were recorded for isolated nanofibres of **1**@GNF or **2**@GNF using an Oxford Instruments X-rays detector at 200 kV.

Insertion of catalysts in GNF.

PdSalen or C_{60}PdSalen (7.5 x 10^{-4} mmol) were dissolved in THF (2 mL) in a Schlenk tube, freshly annealed GNF (5 mg) were then added and the suspension was stirred for 1 hour. The solvent was then slowly removed under reduced pressure to dryness. Fresh THF (2 mL) was then added, and the procedure repeated 5-6 times. The resulting material was allowed to dry under vacuum for 20 h. The composite materials were characterised via TEM and EDX, and utilised in the subsequent catalytic reaction as obtained.

Heck Coupling.

The catalyst (7.5 x 10^{-4} mmol; 5 mg) and Na_2CO_3 (0.3 mmol) were placed in a Schlenk tube and thoroughly degassed with Ar. The aryl bromide (0.15 mmol), aryl alkene (0.3 mmol) and dimethylformamide (0.6 mL) were then added, and the resulting solution was thoroughly degassed by bubbling Ar for 30 minutes then heated at 140˚C for 90 hours. The resulting mixture was then analysed by ^{1}H NMR spectroscopy.

Trans-stilbene*:* ^{1}H NMR (400 MHz, CDCl$_3$): δ=7.15 (s, 2H; CH=CH), δ=7.28-7.33 (m, 2H; Ar), δ=7.36-7.41 (m, 4H; Ar), δ=7.51-7.57 (m, 4H; Ar).

Cis-stilbene*:* ^{1}H NMR (400 MHz, CDCl$_3$): δ=6.62 (s, 2H; CH=CH), δ=7.18-7.27 (m, 10H; Ar).

1,1-Diphenylethylene*:* ^{1}H NMR (400 MHz, CDCl$_3$): δ=5.48 (s, 2H; CH$_2$=C), δ=7.29-7.38 m, 10H; Ar).

1-[(E)-2-Phenylvinyl]naphthalene*:* ^{1}H NMR (400 MHz, CDCl$_3$): δ=7.12 (d, ^{3}J(H, H)=16.1 Hz, 1H, CH=CH)), δ=7.26-7.59 (m, 8H; Ar and CH=CH), δ=7.71-7.88 (m, 4H; Ar), 8.20 (d, 1H, ^{3}J(H,H)=8.2 Hz; Ar).

<u>1-[(Z)-2-Phenylvinyl]naphthalene</u>: ^{1}H NMR (400 MHz, CDCl$_3$): δ=6.83 (d, ^{3}J(H,H)=12.1 Hz 1H, C<u>H</u>=CH), δ=7.04-7.08 (m, 6H; Ar and CH=C<u>H</u>), δ=7.32-7.36 (m, 2H; Ar), δ=7.48-7.50 (m, 2H; Ar), δ=7.76-7.78 (m, 1H; Ar), δ=7.86-7.88 (m, 1H; Ar), δ=8.07-8.09 (m, 1H; Ar).

<u>1-(1-Phenylvinyl)naphthalene</u>. ^{1}H NMR (400 MHz, CDCl$_3$): δ=5.39 (d, ^{2}J(H,H)=1.2 Hz, 1H; C<u>H</u>H=C)), δ=5.98 (d, ^{2}J(H,H)=1.2 Hz, 1H; CH<u>H</u>=C), δ=7.22-7.34 (m, 6H; Ar), δ=7.40-7.51 (m, 3H; Ar), δ=7.76 (d, ^{3}J(H,H)=8.4 Hz, 1H; Ar), δ=7.84-7.87 (m, 2H; Ar).

<u>1-(^{t}Bu)-4-[(E)-2-phenylvinyl]benzene</u>: ^{1}H NMR (400 MHz, CDCl$_3$): δ=1.38 (s, 9H; C(CH$_3$)$_3$), δ=7.08 (s, 2H; CH=CH), 7.24-7.53 (m, 9H; Ar).

<u>1-(^{t}Bu)-4-[(Z)-2-phenylvinyl]benzene</u>: ^{1}H NMR (400 MHz, CDCl$_3$): δ=1.32 (s, 9H; C(CH$_3$)$_3$), δ=6.57 (s, 2H; CH=CH), δ=7.15- 7.26 (m, 9H; Ar).

<u>1-Phenyl 1- (4-^{t}Bu-phenyl) ethylene</u>: ^{1}H NMR (400 MHz, CDCl$_3$, δ): δ=1.38 (s, 9H; C(CH$_3$)$_3$), δ=5.44 (d, ^{2}J(H,H)=1.6 Hz, 1H; C<u>H</u>H=C), δ=5.49 (d, ^{2}J(H,H)=1.6 Hz, 1H; CH<u>H</u>=C), δ=7.26-7.38 (m, 9H; Ar).

<u>(E)-1-Styrylpyrene</u>: ^{1}H NMR (400 MHz, CDCl$_3$): δ=7.31-7.54 (m, 4H, Ar), δ=7.74-7.77 (m, 2H, Ar), δ=8.03-8,27 (m, 8H, Ar), δ=8.36 (d, ^{3}J(H,H)=8.40 Hz, 1H, CH), δ=8.54 (d, ^{3}J(H,H)=8.40 Hz, 1H, CH).

<u>1-Phenyl-1-(1'-pyrenyl)ethylene</u>: ^{1}H NMR (400 MHz, CDCl$_3$, δ): δ=5.49 (d, ^{2}J(H,H)=2Hz, 1H, C<u>H</u>H=C), δ=6.14 (d, ^{2}J(H,H)=2 Hz, 1H, CH<u>H</u>=C), δ=7.2-7.4 (m, 5H, Ar), δ=7.9-8.2 (m, 9H, Ar).

<u>(E)-4-Methoxystilbene</u>: ^{1}H NMR (400 MHz, CDCl$_3$): δ=3.82 (s, 3H, CH$_3$), δ=6.90 (d, J=5.0 Hz, 2H, Ar), δ=6.99 (d, ^{3}J(H,H)=16.5 Hz, 1H, C<u>H</u>=CH), δ=7.08 (d, ^{3}J(H,H)=16.5 Hz, 1H, CH=C<u>H</u>), δ=7.26-7.21 (m, 1H, Ar), δ=7.34 (d, J=7.5 Hz, 2H, Ar), δ=7.49-7.44 (m, 4H).

<u>(Z)-1-Methoxy-4-styrylbenzene:</u> ^{1}H NMR (400 MHz, CDCl₃, δ): δ=3.81 (s, 3H, CH₃), δ=6.56-6.55 (m, 2H), δ=6.79 (d, J=8.8 Hz, 2H), δ=7.30-7.17 (m, 7H, Ar).

<u>1-Methoxy-4-(1-phenylvinyl)benzene:</u> ^{1}H NMR (400 MHz, CDCl₃, δ): δ=3.78 (s, 3H, CH₃), δ=5.34 (d, $^2J(H,H)$=1.2 Hz, 1H, C<u>H</u>H=C), δ=5.38 (d, $^2J(H,H)$=1.2 Hz, 1H, CH<u>H</u>=C), δ=6.84 (d, $^3J(H,H)$=8 Hz, 2H, Ar), δ=7.26 (d, $^3J(H,H)$=8.8 Hz, 2H, Ar), δ=7.32-7.29 (m, 5H, Ar).

Recyclability test.

Heck reactions were performed as described above. After heating the reaction mixture to 140 °C for 90 h the reaction mixture was allowed to cool to room temperature, the catalyst was removed by filtration, washed extensively with cold CH₃CN (20 mL) and dried under vacuum for 20 h. The resulting material was then used in the next otherwise identical catalytic cycle.

Computational details.

The geometry optimization simulations were performed using a molecular mechanics approach. Modified Universal Force Field (UFF_corrected) was used implementing new Lennard-Jones parameters for carbon atoms[32] to UFF,[33] keeping other parameters (bond stretching, angle bending etc.) unchanged (see SI file for details). Partial atomic charges of **1** and **2** were calculated using the Qeq approach.[34] The size of the GNF is shown in Figure S4. Dangling bonds of GNF were saturated by hydrogen atoms. All of the atoms in the GNF were neutral and frozen. Binding energies were calculated as $E_{binding}$=E(**1**@GNF) - E (**1**) - E(GNF) in the case of **1**, and equivalently in case of **2**.

Graphical abstract

Interactions of Pd(II)complexes with a carbon nanoreactor (graphitised nanofiber, GNF) change activity and selectivity of the catalyst. Distribution of isomeric products of a cross-

coupling reaction performed in GNF reveal important role of the carbon nanoreactor in the catalytic cycle, and shed light on the location and orientation of the catalyst molecules inside the GNF channel.
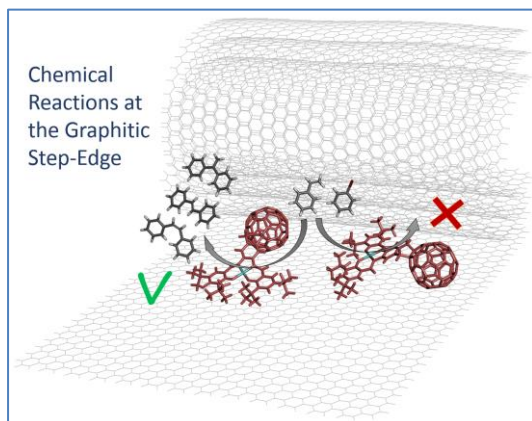
References.

[1] D. E. De Vos, M. Dams, B. F. Sels, P. A. Jacobs, *Chem. Rev*. **2002**, *102*, 3615-3640.

[2] R. Chakrabarty, P. S. Mukherjee, P. J. Stang, *Chem. Rev*. **2011**, *111*, 6810-6918.

[3] (a) P. M.Arnal, M. Comotti, F. Schüth, *Angew. Chem*. **2006**, *118*, 8404-8407; (b) C. Galeano, R. Güttel, M. Paul, P. Arnal, A.-H. Lu, F. Schüth, *Chem. Eur. J*. **2011**, *17*, 8434-8439; (c) J. C. Park, H. J. Lee, J. Y. Kim, K. H. Park, H. J. Song, *Phys. Chem. C*, **2010**, *114*, 6381-6388..

[4] (a) B. Gui, K.-K. Yee, Y.-L. Wong, S.-M. Yiu, M. Zeller, C. Wang, Z. Xu, *Chem. Commun.,* 2015, 51, 6917—6920; (b) M. A. Gotthardt, A. Beilmann, R. Schoch, J. Engelke, W.Kleist, *RSC Adv*., **2013**, 3, 10676–10679.

[5] Y. H. Ng, M. Wang, H. Han, C. L. L. Chai, *Chem. Commun*., **2009**, 5530–5532.

[6] A.N. Khlobystov, *ACS Nano* **2011**, *5*, 9306-9312.

[7] D.A. Britz, A.N. Khlobystov, K. Porfyrakis, A. Ardavan, G.A.D. Briggs, *Chem. Commun*. **2005**, 37-39.

[8] T.W. Chamberlain, J. Biskupek, G.A. Rance, A. Chuvilin, T.J. Alexander, E. Bichoutskaia, U. Kaiser, A.N. Khlobystov, *ACS Nano* **2012**, *6*, 3943-3953.

[9] A. Chuvilin, E. Bichoutskaia, M.C. Gimenez-Lopez, T.W. Chamberlain, G.A. Rance, N. Kuganathan, J. Biskupek, U. Kaiser, A.N. Khlobystov, *Nat. Mater*. **2011**, *10*, 687-692.

[10] R. R. Meyer, J. Sloan, R. E. Dunin-Borkowski, A. I. Kirkland, M. C. Novotny, S. R. Bailey, J. L. Hutchison, M. L. H. Green, *Science* **2000***, 289*, 1324-1326.

[11] T. Fujimori, A. Morelos-Gómez, Z. Zhu, H. Muramatsu, R. Futamura, K. Urita, M. Terrones, T. Hayashi, M. Endo, S.Y. Hong, Y.C. Choi, D. Tománek, K. Kaneko, *Nat. Comm*. **2013**, 4, 1-8; DOI: 10.1038/ncomms3162.

[12] S.A. Miners, G.A. Rance, A.N. Khlobystov, *Chem. Commun*., **2013**, *49*, 5586-5588.

[13] H. Vardhana, F. Verpoort, *Adv. Synth. Catal*. **2015**, *357*, 1351 −1368.

[14] (a) M. M. Smulders, J. R. Nitschke, *Chem. Sci*. **2012**, 3, 785–788; (b) M. Yoshizawa, Y. Takeyama, T. Kusukawa, M. Fujita, *Angew. Chem*. **2002**, *114*, 1403–1405; (c) M. Yoshizawa, Y. Takeyama, T. Okano, M. Fujita, *J. Am. Chem. Soc*. **2003**, *125*, 3243–3247.

[15] (a) H. Yang, L. Zhang, L. Zhong, Q. Yang, C. Li, *Angew. Chem. Int. Ed*. **2007**, *46*, 6861 −6865; (b) B. Li, S. Bai, X. Wang, M. Zhong, Q. Yang, C. Li, *Angew. Chem. Int. Ed*. **2012**, *51*, 11517–11521; (c) M. Shakeri, L. Roiban, V. Yazerski, G. Prieto, R.J. M. Klein Gebbink, P. E. de Jongh, K. P. de Jong, *ACS Catal*. **2014**, *4*, 3791−3796.

[16] (a) A. La Torre, M.C. Gimenéz-Lopez, M.W. Fay, G.A. Rance, W.A. Solomonsz, T.W. Chamberlain, P.D. Brown, A.N. Khlobystov, *ACS Nano* 2012, *6*, 2000-2007; (b) H. Liu, L. Zhang, N. Wang, D.S. Su, *Angew. Chem. Int. Ed*., **2014**, *53*, 12634-12638; (c) E. Castillejos, P.-J. Debouttièrre, L. Roiban, A. Solhy, V. Martinez, Y. Kihn, O. Ersen, K. Philippot, B. Chaudret, P. Serp, *Angew. Chem. Int. Ed*., **2009**, *48*, 2529-2533; (d) W.A. Solomonsz, G.A. Rance, M. Suyetin, A. La Torre, E. Bichoutskaia, A.N. Khlobystov, *Chem. A Eur. J*., **2012**, *18*, 13180-13187; (e) W.A. Solomonsz, G.A. Rance, A.N. Khlobystov, *Small*, **2014**, *10*, 1866-1872; (f) W.A. Solomonsz, G.A. Rance, B. J. Harris, A.N. Khlobystov, *Nanoscale*, **2013**, *5*, 12200-12205; (g) G.A. Rance, W.A. Solomonsz, A.N. Khlobystov, *Chem. Commun*., **2013**, 1067-1069; (h) B. Cornelio, G. A. Rance, M. Laronze-Cochard, A. Fontana, J. Sapi, A. N. Khlobystov, *J. Mater. Chem. A*, **2013**, *1*, 8737–8744; (i) B. Cornelio, A. R. Saunders, W. A. Solomonsz, M. Laronze-Cochard, A. Fontana, J. Sapi, A. N. Khlobystov, G. A. Rance, *J. Mater. Chem. A*, **2015**, *3*, 3918–3927.

[17] T. W. Chamberlain, J. Biskupek, S. T. Skowron, P. A. Bayliss, E. Bichoutskaia, U. Kaiser, A. N. Khlobystov, *Small*, **2015**, *11*, 622-629.

[18] M. Oestreich, The Mizoroki-Heck reaction, **2009**, Wiley.

[19] R.F. Heck, *J. Am. Chem. Soc*. **1971**, *93*, 6896–6901.

[20] M. A. Lebedeva, T. W. Chamberlain, E. S. Davies, D. Mancel, B. E. Thomas, M. Suyetin, E. Bichoutskaia, M. Schröder, A. N. Khlobystov, *Chem. Eur. J.*, **2013**, *19*, 11999-12008.

[21] M. A. Lebedeva, T.W. Chamberlain, M. Schröder and A.N. Khlobystov, *Chem. Mater.*, **2014**, 26, 6461-6466.

[22] T. W. Chamberlain, A.M. Popov, A.A. Knizhnik, G. E. Samoilov, A. N. Khlobystov, *ACS Nano*, **2010**, *4*, 5203-5210.

[23] (a) T.W. Chamberlain, N.R. Champness, M. Schröder, A.N. Khlobystov, *Chem. Eur. J.,* **2011**, *17*, 668-674; (b) J. Fan, T. W. Chamberlain, Y. Wang, S. Yang, A. J. Blake, M. Schröder, A. N. Khlobystov, *Chem. Commun.*, **2011**, *47*, 5696–5698; (c) L. Maggini, M.-E. Füstös, T.W. Chamberlain, C. Cebrián, M. Natali, M. Pietraszkiewicz, O. Pietraszkiewicz, E. Székely, K. Kamarás, L. De Cola, A. N. Khlobystov, D. Bonifazi, *Nanoscale*, **2014**, *6*, 2887–2894.

[24] H. Ulbricht, G. Moos, T. Hertel, *PRL*, **2003**, 095501-1-4.

[25] D.V. Kazachkin, Y. Nishimura, H.A. Witek, S. Irle, E. Borguet, *J. Am. Chem. Soc*. **2011**, *133*, 8191–8198.

[26] (a) Y.Heo, Y.Y. Kang, T. Palani, J. Lee, S. Lee, *Inorg. Chem. Commun*, **2012**, *23*, 1-5; (b) S. K. C. Soh, M. Shamsuddin, *J. Chem.*, **2013**, 1-8; (c) N. T.S. Phan, D.H. Brown, H. Adams, S.E. Spey, P. Styring, *Dalton Trans*. **2004**, 1348-1357.

[27] (a) Y.-M. Liu, Y.-C. Lin, W.-C. Chen, J.-H. Cheng, Y.-L. Chen, G.P.A. Yap, S.-S. Sun, T.-G. Ong, *Dalton Trans.*, **2012**, *41*, 7382–7389; (b) M. Feuerstein, H. Doucet, M. Santelli, *Tetrahedron Lett.*, **2002**, *43*, 2191–2194; (c) K. Pan, S. Noël, C. Pinel, L. Djakovitch, *J. Organomet. Chem.*, **2008**, *693*, 2863–2868; (d) L. Yuan, Y. Xu, X. Hu, G. Yang, Y. Wu, *J. Molec. Cat. A: Chem.*, **2015**, *396*, 55–60.

[28] M. Pagliaro, V. Pandarus, R. Ciriminna, F. Béland, P. D. Cará, *ChemCatChem*, **2012**, *4*, 432 – 445.

[29] (a) K. Köhler, R.G. Heidenreich, J. G. E. Krauter, J. Pietsch, *Chem. Eur. J.* **2002**, *8*, 622-631; (b) S. J. Broadwater, D. T. McQuade, *J. Org. Chem.* **2006**, *71*, 2131-2134; (c) T. J. Colacot, E. S. Gore, A. Kuber, *Organometallics*, **2002**, *21*, 3301-3304; *(d)* M. Pagliaro, V. Pandarus, F. Béland, R. Ciriminna, G. Palmisano, P. D. Cará, *Catal. Sci. Technol.*, **2011**, *1*, 736–739.

[30] (a) I.P. Beletskaya, A.V. Cheprakov, *Chem. Rev*. **2000**, *100*, 3009-3066; (b) A.M. Trzeciak, J.J. Zi´ołkowski, *Coord. Chem. Rev*. **2005**, *249*, 2308–2322; *(c)* N. T. S. Phan, M. Van Der Sluys, C. W. Jones, *Adv. Synth. Catal.* **2006**, *348*, 609 – 679; (d) J. Ruan J. Xiao, *Acc. Chem. Res*. **2011**, *44*, 614–626.

[31] Y.-R. Luo. Handbook of Bond Dissociation Energies in Organic Compounds. CRC *Press*, **2002**, 151-157.

[32] L. Tang, X. Yang, *J. Phys. Chem. C*, **2012**, *116*, 11783.

[33] A. K. Rappe, C. J. Casewit, K. S. Colwell, W. A. Goddard III, W. M. Skid, *J. Am. Chem. Soc.* **1992**, *114*, 10024−10035.

[34] A. K. Rappe, W. A. Goddard, *J. Phys. Chem.*, **1991**, *95*, 335.